

Supporting Information

Shaping and enhancing the photoluminescence of halide perovskite quantum dots with plasmonic lattices.

Elizabeth Mendoza-Sandoval,^a Germán Rodríguez-López,^b Cesar L. Ordóñez-Romero,^a David Ley^a, Naser Qureshi,^d Michal Urbánek,^c Diego Solis-Ibarra,^b Cecilia Noguez,^a Hugo A. Lara-García,^a and Giuseppe Pirruccio.*^a

^aInstituto de Física, Universidad Nacional Autónoma de México, Apartado Postal 20364, Mexico City 01000, México

^bInstituto de Investigaciones en Materiales, Universidad Nacional Autónoma de México, CU, Coyoacán, Ciudad de México 04510, Mexico

^cCEITEC BUT, Brno University of Technology, Brno 61200, Czech Republic

^dInstituto de Ciencias Aplicadas y Tecnología, Universidad Nacional Autónoma de México, CU, Coyoacán, Ciudad de México 04510, Mexico

Experimental Section

Synthesis

The CsPbBr₃ nanocubes were synthesized according to the previously reported protocol (ACS Energy Lett. 2018, 3, 329–334)

Cs-oleate synthesis: In a typical synthesis, 0.6 mmol (162.5 mg) of Cs₂CO₃ (Sigma-Aldrich, 99%) was loaded in a three-neck round bottom flask along with 9 ml of 1-octadecene (Sigma-Aldrich, technical grade, 90%) and 1 ml of oleic acid (Sigma-Aldrich, technical grade, 90%). The reaction mixture was nitrogen purging at 120°C for one hour. Subsequently, the reaction temperature was raised at 150°C for 10 min forming a clear Cs-oleate solution, that was collected under hot conditions and stored in a dry vial.

Oleylammonium bromide synthesis (OLA-HBr): 10 ml of oleylamine (Sigma Aldrich, technical grade, 70%) and 1 ml of HBr (Sigma-Aldrich, ACS reagent, 48%) were loaded in 25 ml three-neck round-bottomed flask, then the reaction mixture was heated at 120°C and nitrogen purging for 2 hours. The final mixture was collected under hot conditions and stored in a dry vial.

Both stock solutions, Cs-oleate and OLA-HBr, are suspensions at room temperature and need to be heated at 80°C and 100°C respectively to solubilize the solutions and then use them for hot- injection.

CsPbBr₃ nanocubes synthesis: In a typical hot-injection synthesis, 0.2 mmol (73.4 mg) of PbBr₂ (Sigma Aldrich, ≥ 98 %) and 5 ml of 1-octadecene (Sigma-Aldrich, technical grade, 90%) were loaded in a 25 ml three-neck round bottom flask, the mixture was nitrogen purging at 120°C for 1 hour, then 0.5 ml of oleylamine (Sigma Aldrich, technical grade,

70%) and 0.5 ml of oleic acid (Sigma-Aldrich, technical grade, 90%) were injected into the reaction flask, the mixture was stirring until all PbBr_2 was fully dissolved. Then 0.2 ml of OLA-HBr at 80 °C and 0.5 ml of Cs-oleate at 100 °C were injected successively. Just after the last injection, the reaction was cool down into an ice bath. Then 5 ml of the crude solution were loaded in a centrifuge tube with 5 ml of acetone (Sigma-Aldrich, HPLC \geq 99.9%) ,and centrifugated at 7000 rpm for 20 min. After centrifugation, the supernatant solution was discarded, and the precipitate was dispersed in Toluene.

PMMA solution: 20 mg of PMMA (MW 350 000) were dissolved in 10 mL of toluene. The solution was heated at 60°C and stirring for a couple of hours until all the PMMA was dissolved.

Thin Film: 30 mg of CsPbBr_3 were added to the PMMA solution. The perovskites were deposited by spin coating at 2000 rpm during 1 min. Afterwards, the thin film was dried at 80°C in a hotplate for 10 min.

Aluminum Plasmonic lattices were fabricated by reactive ion etching of 150 nm Al thin film over hydrogen silsesquioxane (HSQ) resist mask patterned by electron beam lithography. The 150 nm Al film with 9 nm Ti capping layer was grown by magnetron sputtering on microscopy glass slides. After deposition, the samples were spin-coated with 30 nm of HSQ (FOX-16) resist and by conductive coating (Electra 92). Square arrays (0.5 x 0.5 mm²) of circles with a diameter of 80 nm ordered into square and triangular lattices with a pitch ranging from 300 nm to 475 nm were written into the resist by electron beam writer (RAITH 150-2). After development, the sample was etched for 30 s by reactive ion etching at a power of 200 W in a $\text{BCl}_3:\text{Cl}_2$ gas mixture (1:1 gas ratio, pressure 40 mTorr, Oxford Instruments PlasmaPro NGP 80). The resulting structures were 150 nm tall cylinders.

Figures

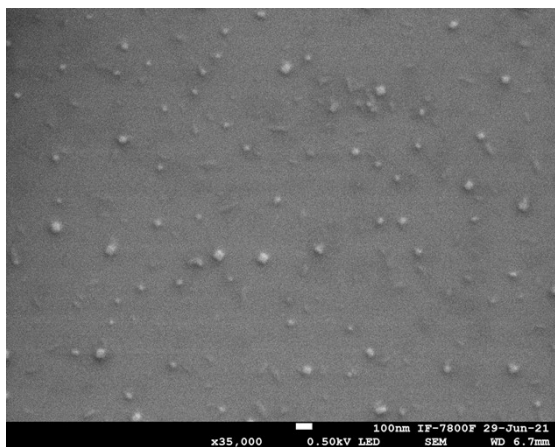


Figure S1. SEM image of the PMMA- CsPbBr_3 thin film.

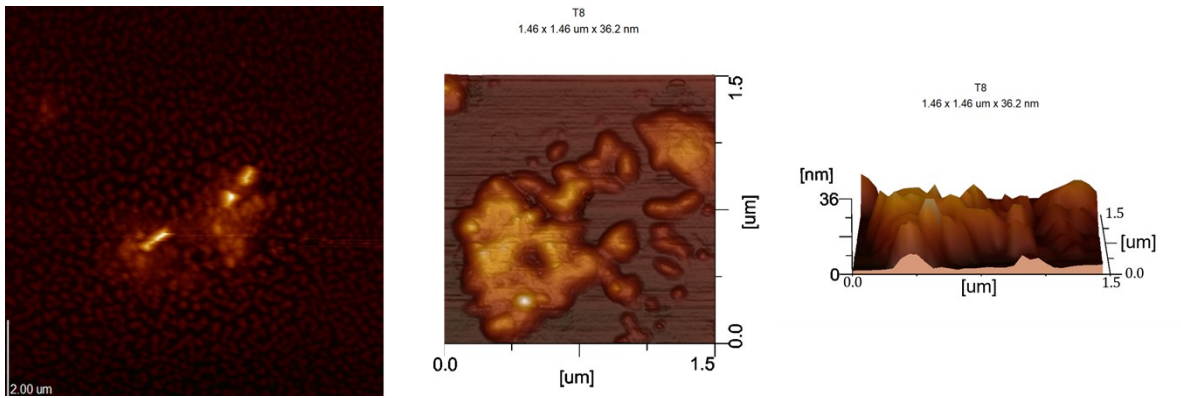


Figure S2. AFM images of the PMMA-CsPbBr₃ thin film.

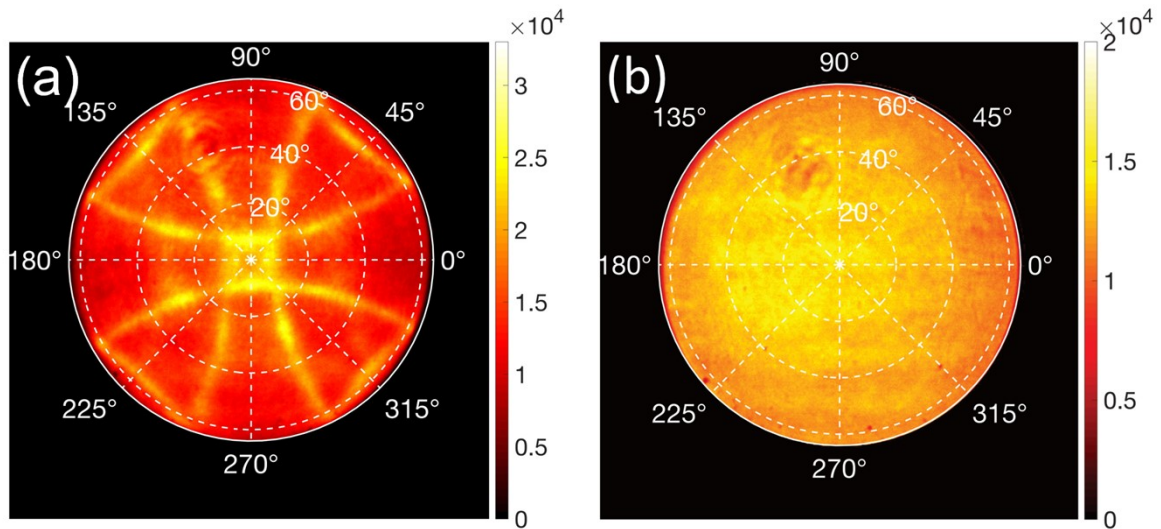


Figure S3. (a) Modified emission spectrum of the PMMA-CsPbBr₃ thin film coupled to the squared plasmonic lattice before normalization. (b) Angular emission of the PMMA-CsPbBr₃ thin film in absence of the plasmonic lattice. The scale is in counts per integration time. Note that the integration times for the two measurements are different.

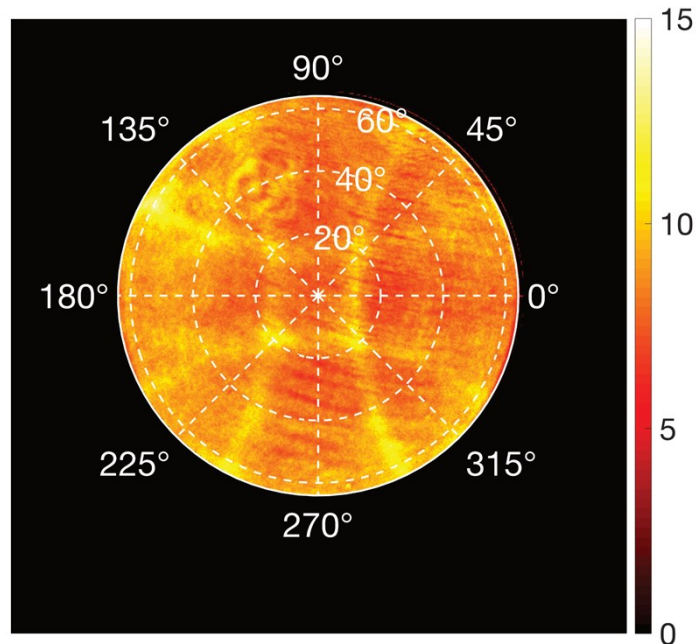


Figure S4. PLE from the PMMA-CsPbBr₃ thin film coupled to the squared plasmonic lattice as a function of the azimuthal and elevation angles for a wavelength of 530 nm.

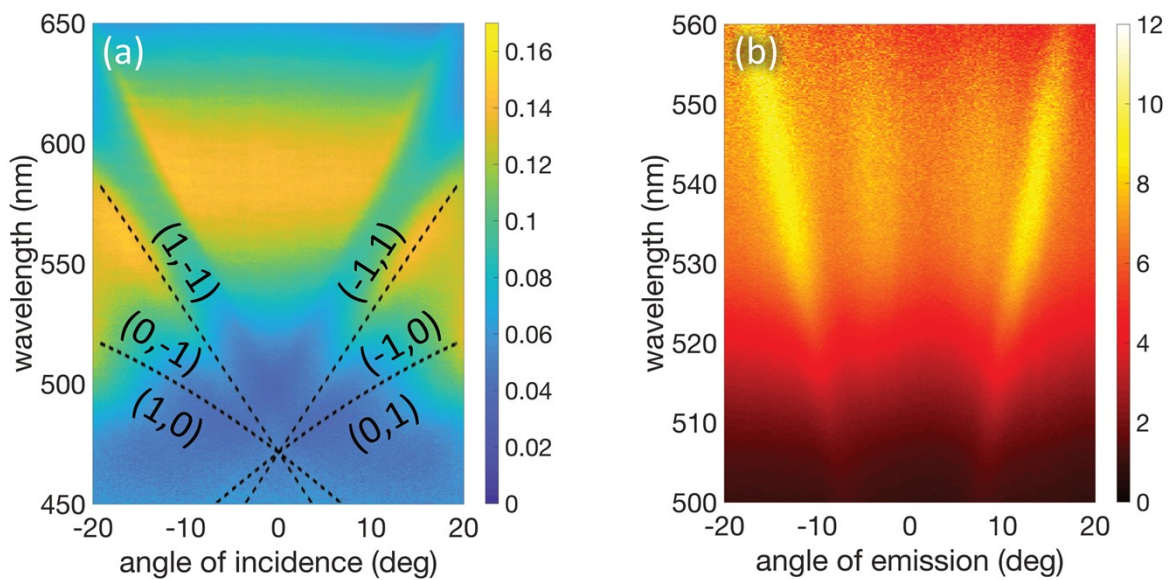


Figure S5. Reflectance (a) and PLE (b) as a function of wavelength and angle of incidence or emission, respectively, for the triangular plasmonic lattice along the Γ -M trajectory. The dashed curves correspond to Rayleigh Anomalies.

Optical Measurements

The angularly and spectrally resolved measurements are obtained by Fourier imaging performed on a homemade optical microscope. This technique maps the back-focal plane of a high numerical aperture microscope objective onto a CCD camera, providing direct information on angular emission [1,2]. In our set-up the sample is illuminated through a Plan Fluor 100x/0.9 NA objective by a near diffraction limited spot. A 473 nm continuous wave laser is used for PL measurements, while a halogen lamp is used for reflectance. To acquire (θ, φ) -resolved reflectance or PL images, the back focal plane of the objective is directly imaged using a Bertrand lens onto a sCMOS camera (Andor Zyla 4.2P). The spectral range is chosen by using band pass optical filters. To acquire wavelength- and angle-resolved spectra, the objective's back focal plane is imaged onto the entrance slit of an imaging spectrograph (Andor Kymera 328i). The collected light is dispersed by a diffraction grating (150 lines mm, blazed at 500 nm) and measured using a sCMOS camera (Andor Zyla 4.2P). A linear polarizer in the collection path is used to select the s- or p-polarization. Switching between real space and reciprocal space images is accomplished by removing the Bertrand lens.

Optical response of the isolated nanocylinder

We simulated the absorption and scattering cross-section of the isolated nanocylinder using COMSOL Multiphysics. The main localized resonance around 400 nm displays a quadrupolar-like density charge distribution. This peak is pronounced and can be excited because of the considerable height of the nanocylinder that allows retardation between the top and the bottom surface of the particle. The intensity of the electric field plotted along the planes crossing the nanocylinder along its diameter and its middle height confirm the expected spatial distribution.

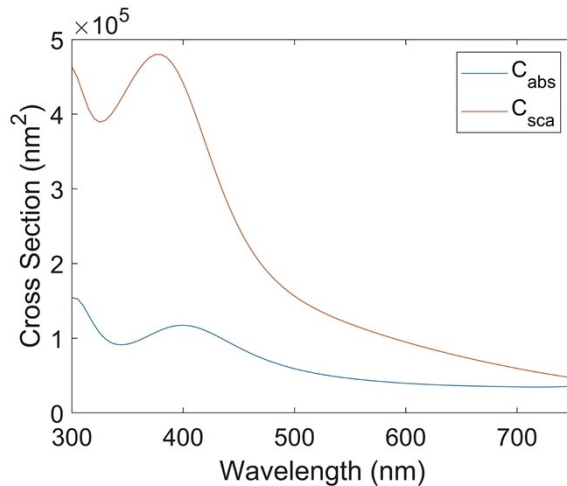


Fig. S6. Normal incidence simulated scattering and absorption cross-section of the isolated nanocylinder.

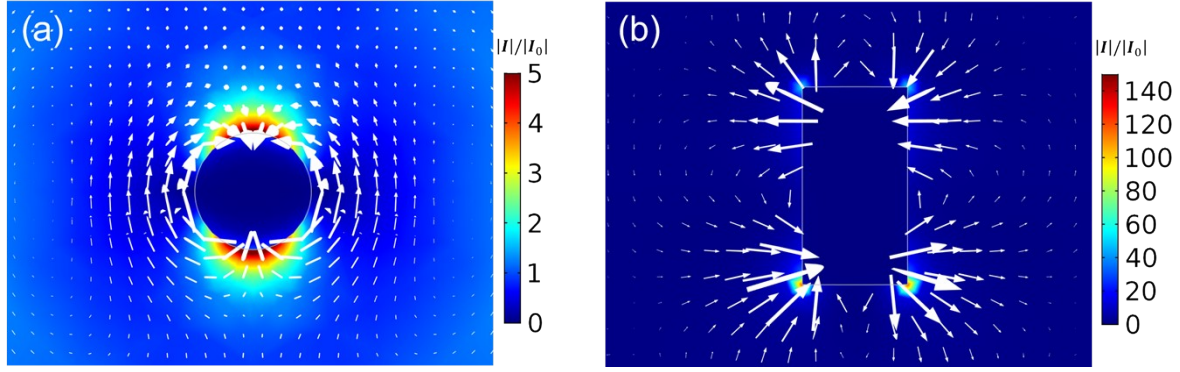


Fig. S7. Normalized electric field intensity for a wavelength of 400 nm plotted along the planes crossing the isolated nanocylinder along its (a) middle height and (b) and its diameter. The vector field corresponds to the scattered electric field.

Optical response of the plasmonic lattices

We simulated the s-polarized reflectance and extinction ($1-T_{00}$, i.e., the zero-th order transmittance) as a function of the incident wavelength and angle for the square and triangular plasmonic lattice along the Γ -X and Γ -M trajectory, respectively. We observe the excitation of a main SLR band associated with the hybridization of the localized resonance with the $(\pm 1, 0)$ diffracted orders for the square lattice and $(1, -1)$, $(-1, 1)$ for the triangular one. In addition to this, additional weak SLRs are present which are associated with the degenerate $(0, \pm 1)$ for the square lattice and the $(0, \pm 1)$, $(\pm 1, 0)$ for the triangular one. Extinction shows the same information but with a larger intensity for the weak modes. The curvature of the SLR band around normal incidence appears smaller for the triangular lattice with respect to the square one. This is due to the interaction of diffractive orders propagating along different directions in the two lattices.

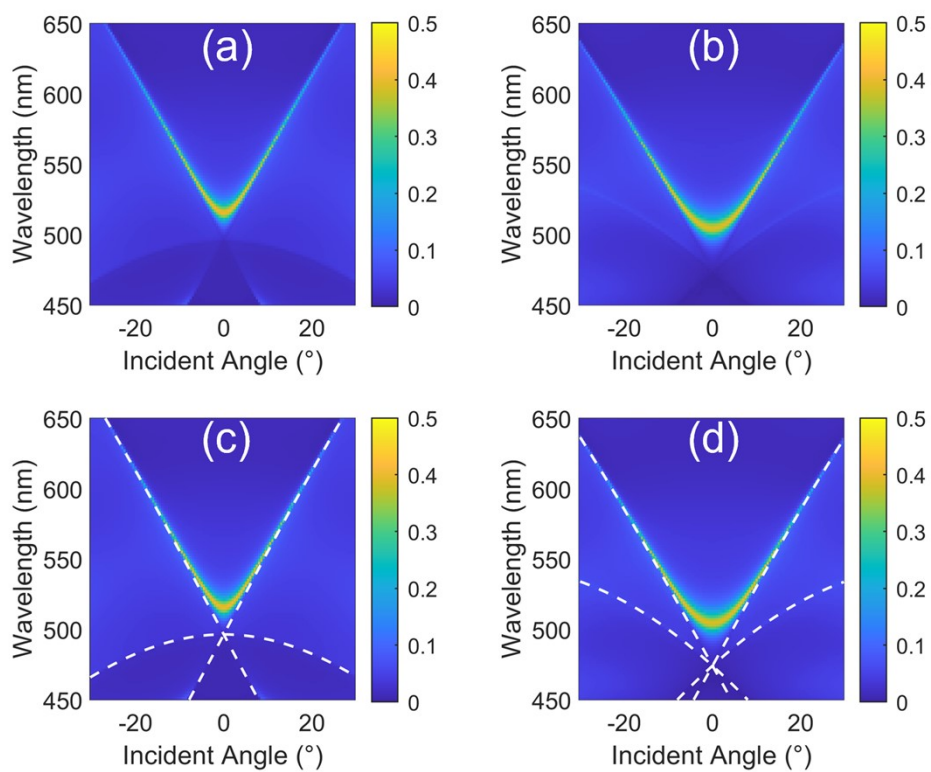


Fig. S8. s-polarized reflectance as a function of the incident wavelength and angle for the (a,c) square and (b,d) triangular plasmonic lattice. The top and bottom row shows the same data in the color plot. The calculated Rayleigh anomalies are plotted with white dashed curves only in the bottom row, for clarity.

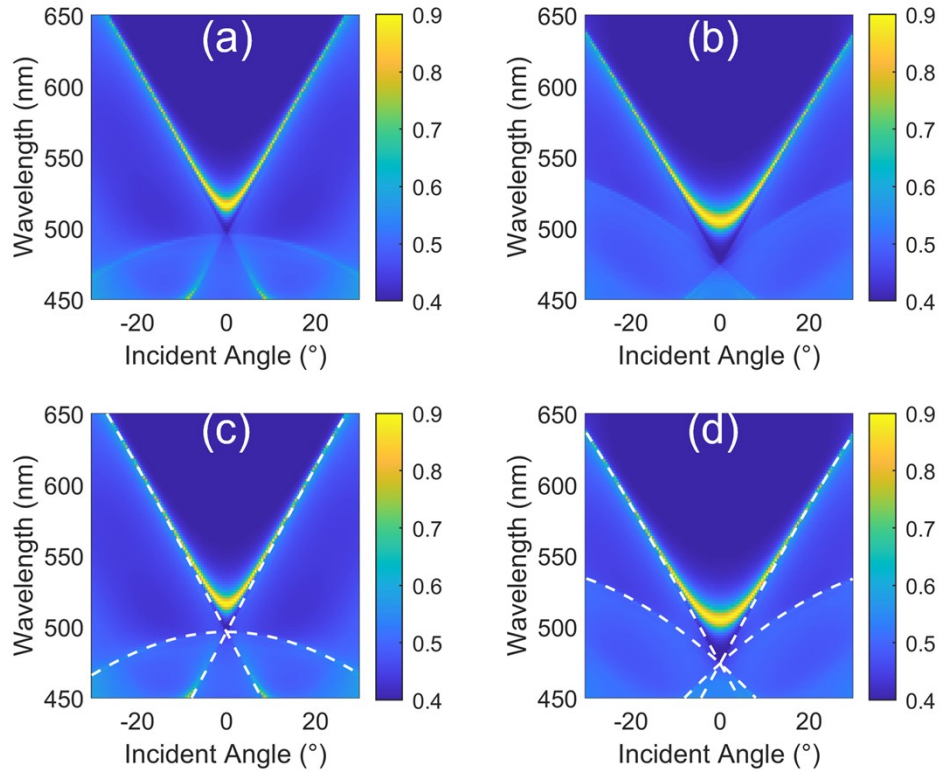


Fig. S9. s-polarized extinction as a function of the incident wavelength and angle for the (a,c) square and (b,d) triangular plasmonic lattice. The top and bottom row shows the same data in the color plot. The calculated Rayleigh anomalies are plotted with white dashed curves only in the bottom row, for clarity.

In Fig. S10 and S11 we plot the normalized intensity of the electric field within the unit cell for the square and triangular lattice, respectively, for the two planes crossing the nanocylinder along its diameter and its middle height. In both cases the scattered electric field displayed as a vector field is superposed. The fields are calculated for the SLR peak at normal incidence of the two lattices. These figures demonstrate the predominantly dipolar nature of the main SLR bands. The dipolar symmetry of the main SLR band is due to the detuning from the quadrupolar scattering cross-section peak (Fig. S5) and to the plane wave-like diffractive orders driving each nanocylinder. Higher orders SLR are also possible with these lattices [28].

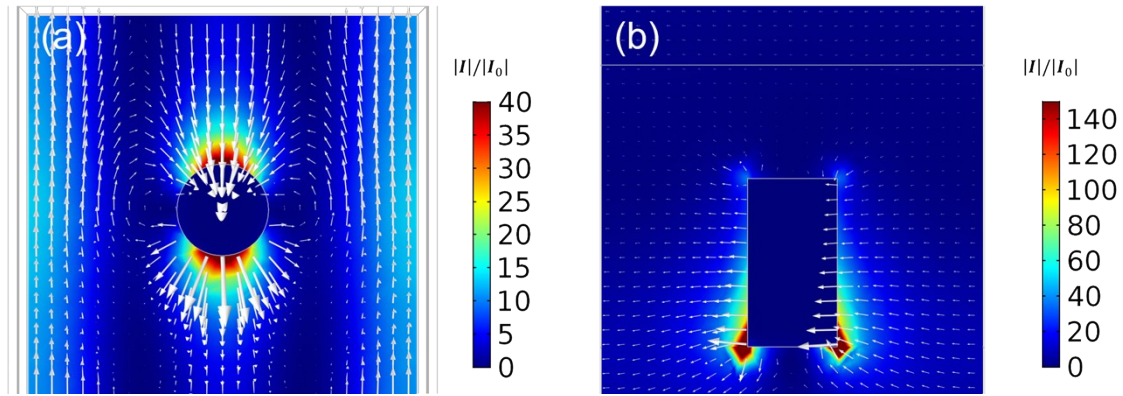


Fig. S10. Normalized electric field intensity within the unit cell for the square lattice for the plane crossing the nanocylinder along its (a) middle height and (b) and its diameter. The vector field corresponds to the scattered electric field.

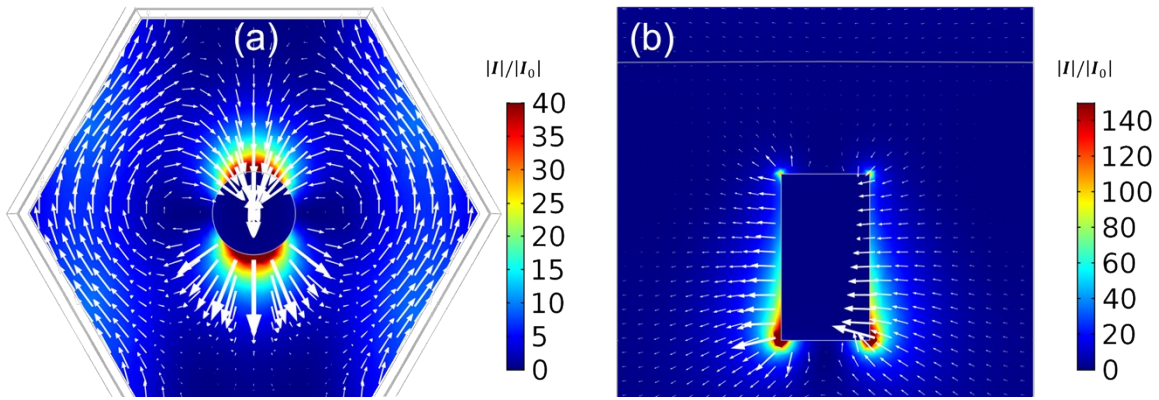


Fig. S11. Normalized electric field intensity within the unit cell for the triangular lattice for the plane crossing the nanocylinder along its (a) its middle height and (b) diameter. The vector field corresponds to the scattered electric field.

The optical band structure of the plasmonic lattices can be modified by changing the lattice parameter. In Fig. S12 we show the s-polarized reflection for the square lattice as a function of the wavelength and angle of incidence for different lattice parameters. Rayleigh Anomalies are displayed as white dashed curves. Besides the spectral narrowing of the SLR, we see that the optical band structure stays the same as we increase the lattice parameter. The controllable SLR redshifts can be used as an effective way to adapt the plasmonic lattices to quantum dots emitting in different part of the visible spectrum. The SLR narrowing is due to the detuning from the localized resonance of the isolated nanocylinder.

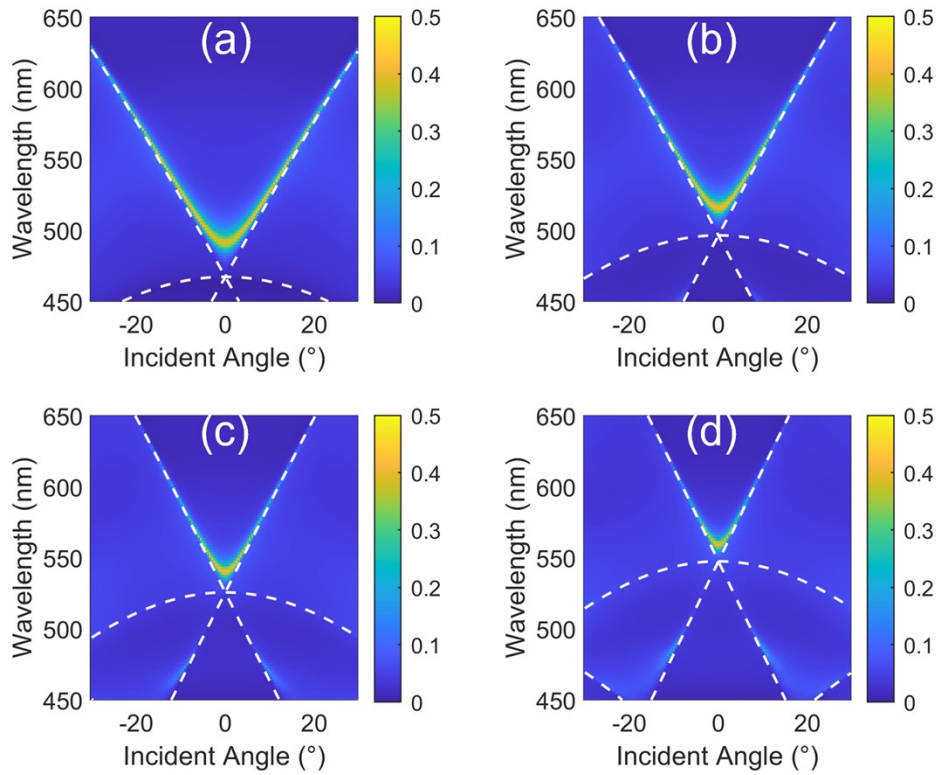


Fig. S12. s-polarized reflection for the square lattice as a function of the wavelength and angle of incidence for lattice parameters equal to (a) 320 nm, (b) 340 nm, (c) 360 nm and (d) 380 nm. The dashed curves correspond to the calculated Rayleigh Anomalies.

[1] J. A. Kurvits, M. Jiang, R. Zia, *J. Opt. Soc. Am. A*, 32:2082–92 (2015).

[2] I. Sersic *et al*, *New J. Phys.* **13** 083019 (2011)